

Comparison of Theoretical Models of Ripple Formation on the Surface of Icicles with Experiments

K. Ueno¹, M. Farzaneh¹ and S. Yamaguchi²

¹NSERC/Hydro-Quebec/UQAC Industrial Chair on Atmospheric Icing of Power Network Equipment (CIGELE) and Canada Research Chair on Atmospheric Icing Engineering of Power Networks (INGIVRE) <http://www.cigele.ca> at the Université du Québec à Chicoutimi, Chicoutimi, QC, Canada

²Snow and Ice Research Center, National Research Institute for Earth Science and Disaster Prevention, Nagaoka, 940-0821, Japan

Abstract—The interaction of fluid flow in a bulk liquid with phase transformation at the solid-liquid interface can create new frontal instabilities. In the absence of flow in the liquid, it is well known that the fundamental building block of the morphological instability of a solidification front is the Mullins-Sekerka theory, which gives conditions for the growth of infinitesimal disturbances of a solid-liquid interface. However, little is known about morphological instability of solidification front in crystal growth from a thin film of flowing liquid. One such example is ring-like ripples on icicles. The ripples always measure about one cm from peak to peak. The water film covering the surface of icicles is very thin, with a water-air surface on one side and growing ice on the other. This is one of the more complicated moving boundary problems with phase transition. Recently, Ogawa and Furukawa developed an initial theoretical model that explains the surprisingly universal structures of ripples on icicles. A completely different ripple formation mechanism has been proposed by the author herein (Ueno). In this new morphological instability theory, the influence of the shape of the liquid-air surface on the growth conditions of disturbances of the solid-liquid interface was taken into account for the first time. In a cold room at a temperature below zero degrees, we experimentally produced a ripple pattern of ice on the surface of a round wooden stick and that of a gutter on an inclined plane at various angles with regard to the horizontal plane, and water was supplied at various rates from their tops. The purpose of this paper is to compare some of the predictions derived from two theories with experimental results.

I. INTRODUCTION

ICICLES grow when they are covered with supercooled water and most of the latent heat is released through the film into the ambient air below 0 °C. During icicle growth, ring-like ripples are often observed on the surface of icicles, as shown in Fig. 1. The wavelength of ripples for natural icicles is always around one centimeter [1]. Although this is a familiar phenomenon for people in cold regions, the ripple formation mechanism is still not well understood.

The Mullins-Sekerka (MS) theory predicts the wavelength of the most unstable mode from the maximum growth rate for initial disturbances [2]. At a convex part indicated by A in Fig. 2 (a), latent heat escapes more easily by diffusion because the temperature gradient at the bulge surface area is large, hence this part grows fast. While, a concave part indicated by B in Fig. 2 (a) grows slowly because the temperature gradient is small. According to the Gibbs-Thomson (GT) effect, the

temperature of the convex part A is depressed by $\Delta T = T_m - T_i$ due to the curvature of the solid-liquid interface, as shown in Fig. 2 (b). Therefore the growth rate of this bulge part becomes smaller because the degree of supercooling reduces from $T_m - T_\infty$ to $T_i - T_\infty$. Here T_m , T_i and T_∞ are the equilibrium melting temperature, the solid-liquid interface temperature at point A, and temperature at infinity, respectively. This tendency counteracts the enhanced freezing at the bulges. As a result of competition between destabilization due to thermal diffusion and stabilization due to the GT effect, a pattern with a specific wavelength of $\lambda_{MS} \approx 2\pi\sqrt{3l_d d_0}$ is developed, as in Fig. 2 (c) [3], [4].

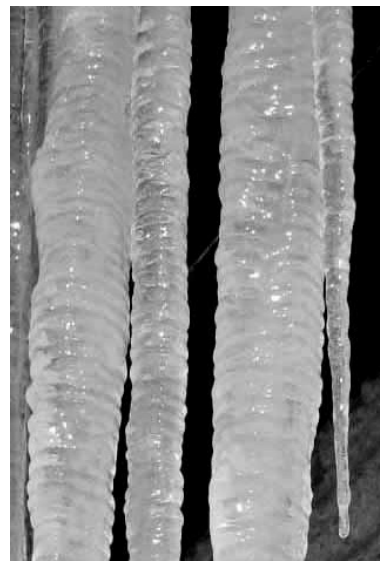


Fig. 1. Ripples on icicles hanging from the roof (air temperature: -10 °C; wind: 0 km/h; 10:00 a.m., Feb 25, 2009, Chicoutimi, Canada).

It should be noted that λ_{MS} contains the thermal diffusion length $l_d = \kappa_l / \bar{V}$ and the capillary length $d_0 = T_m \Gamma C_{pl} / L^2$ associated with the solid-liquid interface tension Γ , where \bar{V} is the mean crystal growth velocity and κ_l is the thermal diffusivity of the liquid, C_{pl} is the specific heat at constant pressure of the liquid, and L is the latent heat of solidification

per unit volume. l_d is the thickness of an accumulation layer of the latent heat released by solidification, as shown in Fig. 2 (b). l_d is usually of macroscopic length, which is about 10 cm in the case of water and for $\bar{V} \sim 10^{-6}$ m/s. On the other hand, d_0 is a microscopic length of the order of angstroms. Hence, λ_{MS} is in the order of microns [3], [4].

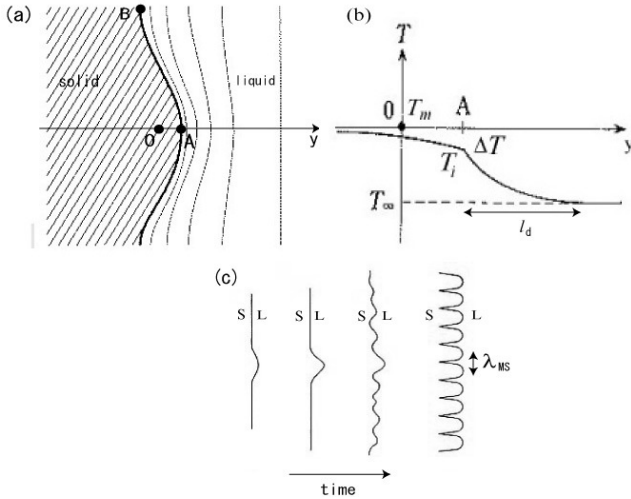


Fig. 2. Schematic illustration of the Mullins-Sekerka instability.

We often see traveling waves of a thin water layer on an inclined substrate as in Fig. 3 (a). The stability analysis of a laminar flow of such a viscous liquid running down an inclined plane was examined [5]. In this case, as shown schematically in Fig. 3 (b), one side of the liquid film is a free surface and the other side is a rigid plane. During the growth of an icicle, a thin film of water from melting snow and ice above the icicle flows along the hanging shaft and refreezes onto the its surface. However, it should be noted that during the liquid flow accompanying a phase transition, the solid-liquid interface may not remain flat when a morphological instability occurs as in Fig. 3 (c). As a result, the flow in the liquid film can change depending on the shape of the solid-liquid interface.

There are some critical differences in situations between Fig. 2 (a) and Fig. 3 (c). The liquid region is assumed to be semi-infinite in Fig. 2 (a) while the liquid in Fig. 3 (c) is a flowing water film with a free surface. In the latter case, we cannot neglect the effect of disturbances of the water-air surface on the growth conditions of disturbances on the ice-water interface. Since the typical thickness of water film flowing down the surface of icicles is about 100 μ m, the thermal diffusion layer cannot be formed in the water film. Furthermore, we do not need to consider the GT effect because the temperature depression due to the curvature effect can be neglected for the typical wavelength of ripples on icicles. Therefore, we have to consider different characteristic lengths from l_d and d_0 in the MS theory, and to develop a quite new mechanism for ripple formation on icicles.

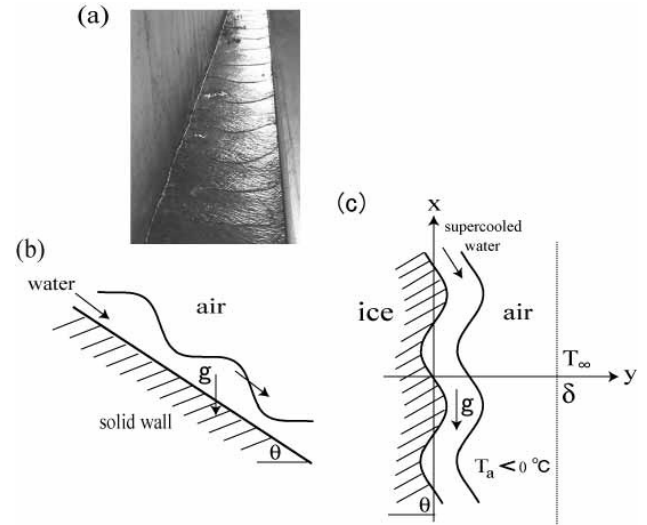


Fig. 3. (a) Waves running down an inclined substrate. (b) and (c) are schematic views of a water film flowing down along a substrate to the horizontal at angle θ driven by gravity. g is the gravitational acceleration (b) is the water flow on the rigid plane and (c) is the ice growth from a thin film of flowing supercooled water. The air temperature, T_a , is below 0°C and $T_a = T_\infty$ at a distance of δ from the flat water-air surface. Since the actual thickness of the water film is very thin compared to the typical wavelength of ripples, we draw the thickness of water film exaggeratedly.

An initial theoretical attempt to explain ripple formation on icicles was recently made [6]. According to their stability analysis of the ice-water interface, the instability of the ice-water interface occurs by the Laplace instability due to thermal diffusion into the air: the latent heat is more rapidly lost from the convex surfaces than that from the concave surfaces in Fig. 3 (c). This makes ice grow faster on the convex protrusions of an icicle than on the concave indentations [6], [7]. And flow in the thin water film makes the temperature distribution uniform, which inhibits the Laplace instability. Using a mathematical model for the competition between those trends, they calculated that the spacing between bulges for any icicle should be 5 to 13 mm. They also predicted that the ripples should migrate downward.

A quite different ripple formation mechanism was proposed by the author herein [8]-[10]. At the inclination angle of $\theta = \pi/2$, the author derived a formula to determine the wavelength of ripples: $\lambda \approx 2\pi(a^2 h_0 Pe_l / 3)^{1/3}$, where $a = [\gamma / (\rho_l g)]^{1/2}$ is the capillary length associated with the surface tension γ of the ice-water interface [11], ρ_l the density of water, and Pe_l the Peclet number which is the ratio of heat transfer due to water flow to that due to thermal conduction in the water film. The author also predicted that the ripples should migrate upward.

The analytical calculations to solve the governing equations with appropriate boundary conditions in these previous papers were very complicated and cumbersome despite the fact that

many approximations were used. The purpose of this paper is to compare the results obtained from the two theories by solving equations numerically with no approximations, and to verify the validity of the theoretical predictions by experiments.

II. THEORY

The theoretical analysis is assumed to be restricted to two-dimensional vertical cross-sections (x, y) , as shown in Fig. 3 (c). The x -axis is parallel to the inclined plane, and the y -axis is normal to it. In the case of laminar flow, h_0 can be expressed by $h_0 = [3\nu_l / (g \sin \theta) Q / l]^{1/3}$ [5], [11], where ν_l is the kinematic viscosity of water, g , the gravitational acceleration, Q / l [ml/h/cm], the water supply rate per width from the top, and θ is the angle of the inclined plane. For typical values of Q / l [1], h_0 is $\sim 100 \mu\text{m}$. For simplicity, we assume that the region of ice is regarded as extending to semi-infinite because the water film is very thin, and that there is no airflow ahead of the water-air surface.

Since there is no noticeable azimuthal variation on the ring-like ripples, as in Fig. 1, we assume only a one-dimensional perturbation of the ice-water interface in the x direction: $\zeta(t, x) = \zeta_k \exp[\sigma t + ikx]$, where k is the wave number and $\sigma = \sigma^{(r)} + i\sigma^{(i)}$, with $\sigma^{(r)}$ being the amplification rate and $v_p \equiv -\sigma^{(i)} / k$ being the phase velocity of the perturbation, and ζ_k is a small amplitude of the ice-water interface. The calculation is based on a linear stability analysis taking into account only the first order of ζ_k [8].

Since the theoretical framework in the absence of airflow is the special case of that described in paper [12], we omit the detailed derivation of the dispersion relation for disturbances of the ice-water interface. The real and imaginary parts of the dispersion relation yield the dimensionless amplification rate $\sigma_*^{(r)} \equiv \sigma^{(r)} / (\bar{V} / h_0)$ and the dimensionless phase velocity $v_{p*} \equiv -\sigma^{(i)} / (k\bar{V})$, respectively,

$$\sigma_*^{(r)} = -\left. \frac{dH_l^{(r)}}{dy_*} \right|_{y_*=0} + n\mu_l (H_l^{(r)}|_{y_*=0} - 1), \quad (1)$$

$$v_{p*} = -\frac{1}{\mu_l} \left(-\left. \frac{dH_l^{(i)}}{dy_*} \right|_{y_*=0} + n\mu_l H_l^{(i)}|_{y_*=0} \right), \quad (2)$$

where $y_* = y / h_0$, $\mu_l \equiv kh_0$, $n = K_s / K_l$ is the ratio of the thermal conductivity of ice to that of water, \bar{V} is the mean growth rate of ice in the normal direction. $H_l^{(r)}$ and $H_l^{(i)}$ are the real and imaginary parts of the amplitude H_l of the perturbed part of temperature in the water film, which is governed by [8]

$$\frac{d^2 H_l}{dy_*^2} = (\mu_l^2 + i\mu_l Pe_l \bar{U}_{l*}) H_l - i\mu_l Pe_l \frac{d\bar{T}_{l*}}{dy_*} f_l, \quad (3)$$

where $\bar{U}_{l*}(y_*) = -(2y_* - y_*^2)$ is the dimensionless velocity profile in the water film in the unperturbed state, which is derived from the no-slip condition at the ice-water interface and the free shear stress at the water-air surface [5], [11]. We note that the sign of \bar{U}_{l*} is opposite to that found in the previous papers [8]-[10] because the direction of the x axis in Fig.3 (c) is opposite. $\bar{T}_{l*}(y_*) \equiv (\bar{T}_l(y_*) - T_{sl}) / (T_{sl} - T_{la}) = -y_*$ is the dimensionless temperature profile of the water film in the unperturbed state. T_{sl} and T_{la} are the temperature of the ice-water interface and that of the water-air surface, respectively. $Pe_l \equiv u_{l0} h_0 / \kappa_l = 3Q / (2l\kappa_l)$ is the Peclet number, u_{l0} being the surface velocity of the water film. f_l on the right hand side of (3) is the amplitude of the perturbed part of the stream function in the water film and is governed by the Orr-Sommerfeld equation [8]:

$$\frac{d^4 f_l}{dy_*^4} = (2\mu_l^2 + i\mu_l Re_l \bar{U}_{l*}) \frac{d^2 f_l}{dy_*^2} - \left\{ \mu_l^4 + i\mu_l Re_l \left(\mu_l^2 \bar{U}_{l*} + \frac{d^2 \bar{U}_{l*}}{dy_*^2} \right) \right\} f_l, \quad (4)$$

where $Re_l \equiv u_{l0} h_0 / \nu_l = 3Q / (2l\nu_l)$ is the Reynolds number.

In the absence of airflow, (34) in [12] reduces to $d^2 H_a / dY_*^2 = \mu_a^2 H_a$, where $\mu_a \equiv k\delta_0$, δ_0 is a length scale characterizing the thickness of thermal boundary layer. With the boundary conditions $H_a|_{Y_*=0} = 1$ and $H_a|_{Y_*=\infty} = 0$, the solution is $H_a = \exp(-\mu_a Y_*)$. Therefore, the perturbed part of the air temperature gradient at the water-air surface defined by (35) in [12] yields $G'_a \equiv h_0 / \delta_0 (-dH_a / dY_*|_{Y_*=0}) = \mu_l$. Hence, the boundary conditions for H_l in (39) and (40) in [12] and those for f_l can be expressed as

$$\begin{aligned} H_l|_{y_*=1} &= -f_l|_{y_*=1} / \bar{U}_{l*}|_{y_*=1}, \\ dH_l / dy_*|_{y_*=1} &= \mu_l f_l|_{y_*=1} / \bar{U}_{l*}|_{y_*=1}, \end{aligned} \quad (5)$$

and

$$\begin{aligned} f_l|_{y_*=0} &= 0, & \left. \frac{df_l}{dy_*} \right|_{y_*=0} &= -\left. \frac{d\bar{U}_{l*}}{dy_*} \right|_{y_*=0}, \\ \left. \frac{d^2 f_l}{dy_*^2} \right|_{y_*=1} &= \left(\left. \frac{d^2 \bar{U}_{l*}}{dy_*^2} \right|_{y_*=1} / \bar{U}_{l*}|_{y_*=1} - \mu_l^2 \right) f_l|_{y_*=1}, \\ \left. \frac{d^3 f_l}{dy_*^3} \right|_{y_*=1} &= (i\mu_l Re_l + 3\mu_l^2) \left. \frac{df_l}{dy_*} \right|_{y_*=1} - i(\alpha / \bar{U}_{l*}|_{y_*=1}) f_l|_{y_*=1}, \end{aligned} \quad (6)$$

where $\alpha = 2(\cot \theta)\mu_l + 2 / \sin \theta (a / h_0)^2 \mu_l^3$, in which the effect of restoring forces due to surface tension and gravity force on the water-air surface is included [8], [10].

III. COMPARISON OF TWO THEORETICAL MODELS

Decomposing H_l and f_l into the real parts $H_l^{(r)}$, $f_l^{(r)}$ and the imaginary parts $H_l^{(i)}$, $f_l^{(i)}$ and noting that $\bar{U}_{l*}|_{y_*=-1} = -1$, $d\bar{U}_{l*}/dy_*|_{y_*=0} = -2$ and $d^2\bar{U}_{l*}/dy_*^2|_{y_*=-1} = 2$, we solve numerically (3) and (4) with boundary conditions (5) and (6) without using the long wavelength approximation. The results are shown by the solid lines in Figs. 4 (a) and (b). Our amplification rate $\sigma_*^{(r)}$ in Fig. 4 (a) acquires a maximum value at $\mu_l = 0.061$. This is the most unstable mode of disturbance of the ice-water interface, from which we define the wavelength of ripple. Since the wave number k is normalized by h_0 , the corresponding wavelength is 9.4 mm from $\lambda = 2\pi h_0 / \mu_l$ for $Q/l = 50$ [(ml/cm)/h] and $\theta = \pi/2$. At $\mu_l = 0.061$, the magnitude of phase velocity is $v_{p*} = 0.59$ from Fig. 4 (b). As shown in Fig. 4 (c), the amplitude of an initial infinitesimal disturbance increases and moves upward with time. It should be noted that this picture cannot be understood by the Mullins-Sekerka or the Laplace instability.

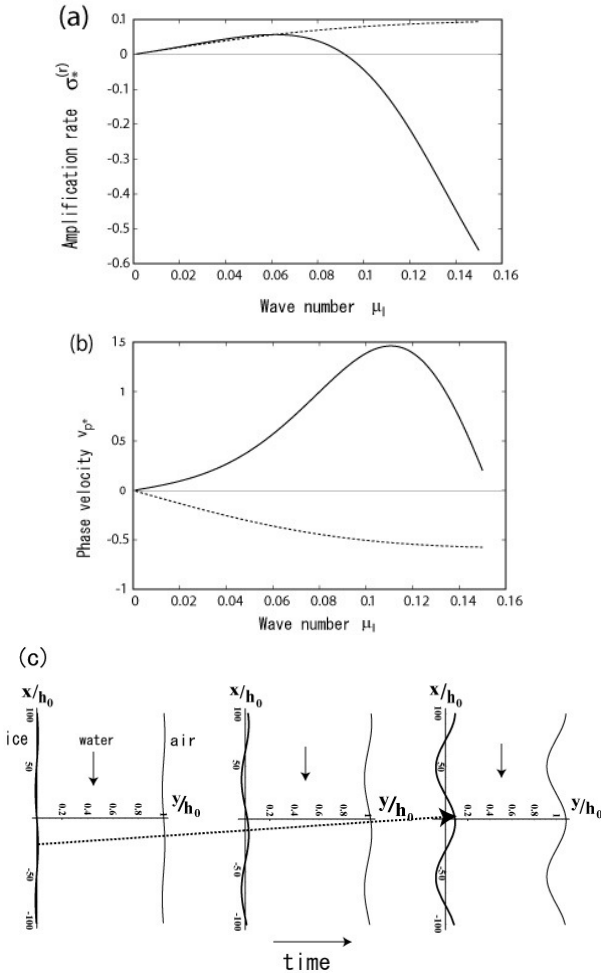


Fig. 4. For $Q/l = 50$ [(ml/h)/cm] and $\theta = \pi/2$, (a) represents dimensionless amplification rate $\sigma_*^{(r)}$ versus dimensionless wave number μ_l , (b)

represents dimensionless phase velocity v_{p*} versus dimensionless wave number μ_l . Solid lines in (a) and (b) are numerical results with the boundary conditions in [8]; dashed lines are numerical results calculated by us with the boundary conditions in [6]. (c) Schematic illustration of time development of an initial disturbance of the ice-water interface.

The main difference between the model found in [6] and [8] is found in the different boundary conditions. In the Ogawa model, the continuity conditions $T_l|_{y=\zeta} = T_s|_{y=\zeta} = T_m$ at the ice-water interface were adopted, where T_m is the equilibrium freezing temperature. This corresponds to the condition $H_l|_{y_*=0} = 1$ in our theoretical framework. They also neglected the effect of restoring forces on the water-air surface.

In order to check the validity of the approximations used in the model found in [6], we solve numerically the same ordinary differential equations with the boundary conditions by replacing only the first equation in (5) with $H_l|_{y_*=0} = 1$, and by neglecting the effect of restoring force, e.g. putting $\alpha = 0$ in the last equation in (6). The results are shown by the dashed line in Figs. 4 (a) and (b). Our numerical calculation shows that the length scale of ripples cannot be determined from their model because $\sigma_*^{(r)} > 0$ for any wave number. This indicates that the ice-water interface does not have any stability mechanism. Therefore, we cannot accept the analytical results in [6] and the corresponding interpretation for the ripple formation mechanism.

IV. EXPERIMENTAL RESULTS

We experimentally produced ripple pattern similar to icicles on an inclined wooden gutter on a plane (Fig. 5 (a)) and a wooden round stick (Fig. 5 (b)) with a length of $l_x = 80$ cm in a cold room. Water was pumped from the reservoir and dripped from the tip of the silicon tube at the rate Q ml/h. The temperature of the dripping water was controlled to be slightly above 0°C .

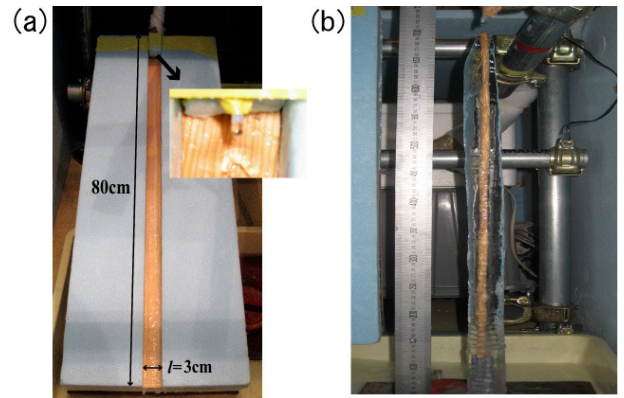


Fig. 5. (a) is an inclined gutter 80 cm in length, $l = 3$ cm in width and 2.5 cm in depth. (b) is a stick 80 cm in length and 6mm in diameter. Water drips from the tip of the silicon tube covered with a band heater at the water supply rate Q ml/hr and flows down along the gutter and stick.

All instruments were set in a box, as shown in Fig. 6 (a), and were protected by a heating device in order to prevent the

water from freezing in the silicon tube. In the absence of a cover of the box, large temperature fluctuations between $-4\text{ }^{\circ}\text{C}$ and $-13\text{ }^{\circ}\text{C}$ were observed in the box, as shown in Fig. 6 (c). This is due to the three ceiling fans of the cold room seen in Fig. 6 (b). These fans keep the temperature in the cold room uniform by automatically switching on and off periodically. On the other hand, in the presence of the cover on the box, the temperature fluctuations were reduced to between $-7\text{ }^{\circ}\text{C}$ and $-9\text{ }^{\circ}\text{C}$, as shown in Fig. 6 (c). Our experiments were conducted with the large temperature fluctuations because ice appears to grow faster when there is air movement. Figure 6 (d) shows the radius growth rate \bar{V} of icicles produced on the 6 mm-diameter round stick against various water supply rates. It is found that it is almost independent of the water supply rate. The mean value is 1.7 mm/h.

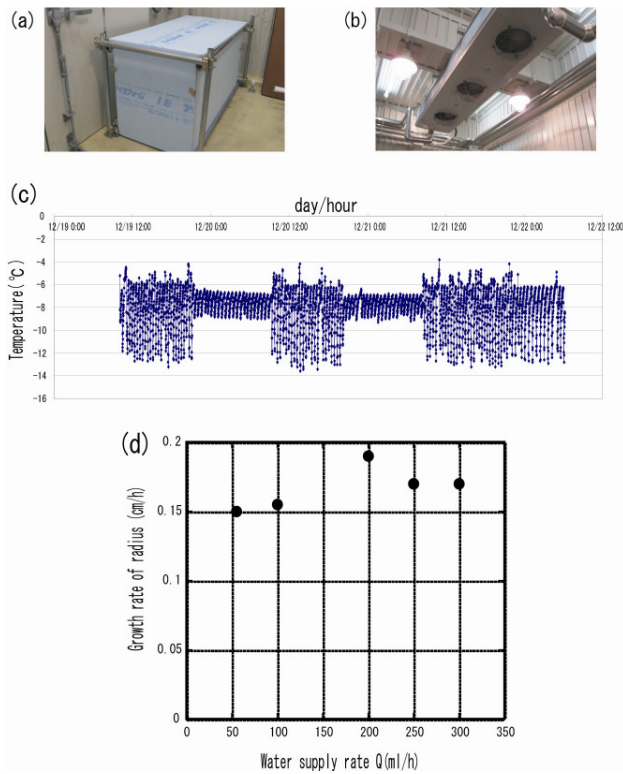


Fig. 6. (a) A box with a cover in a cold room. (b) Fans equipped with the ceiling of the cold room. (c) Temperature fluctuations in the box. Large and small fluctuations are in the absence and presence of the cover of the box, respectively. (d) The radius growth rate \bar{V} of icicles produced on a round stick at various water supply rates Q .

A portion of the supplied water freezes and the rest flows down the ice surface. Therefore, Q/l in h_0 , Pe_l and Re_l should be replaced by $Q/l - (\rho_s / \rho_l) \bar{V} l_x$ from the mass conservation, where ρ_s and ρ_l are the densities of ice and water, respectively. The theoretical curves in Figs. 7 and 8 were obtained using the values of $\rho_s / \rho_l = 0.9$, $l_x = 80$ cm and $\bar{V} = 1.7$ mm/h under the assumption that ice is completely produced along the gutter on a plane, from top to bottom.

The solid and dashed lines in Fig. 7 (c) shows the theoretical dependence of the wavelength of ripples on the angle of the inclined plane at $160/3 - (\rho_s / \rho_l) \bar{V} l_x$ [(ml/h)/cm] and $100 - (\rho_s / \rho_l) \bar{V} l_x$ [(ml/h)/cm], respectively. Figs. 7 (a) and (b) show the ripples of ice produced on the gutter at small and large angles, respectively. The experimental results (Δ and \bullet) at $Q/l = 160/3$ [(ml/h)/cm] in Fig. 7 (c) show that the wavelength of ripples increases with a decrease in angle, which is in good agreement with the theoretical result at $160/3 - (\rho_s / \rho_l) \bar{V} l_x$ [(ml/h)/cm] (solid line) except for the small angle.

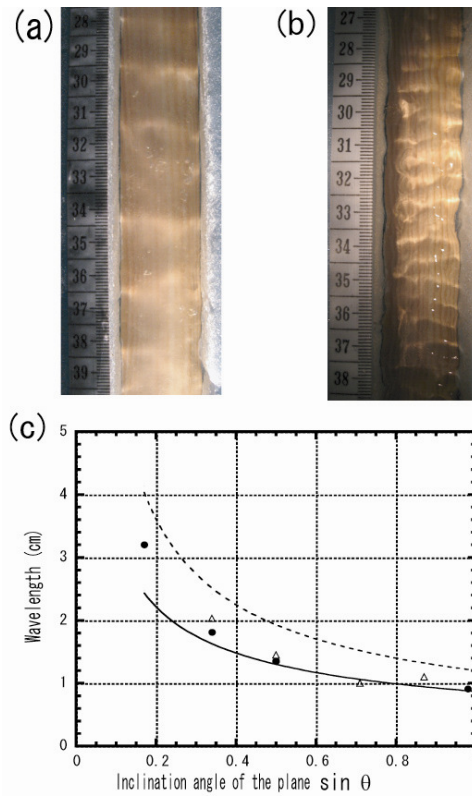


Fig. 7. (a) and (b) are ripples produced on the gutter at small and large angles, respectively. (c) The wavelength of ripples versus $\sin \theta$ at $160/3 - (\rho_s / \rho_l) \bar{V} l_x$ [(ml/h)/cm] (solid line) and $100 - (\rho_s / \rho_l) \bar{V} l_x$ [(ml/h)/cm] (dashed line). Δ and \bullet are experimental result at $Q/l = 160/3$ [(ml/h)/cm] by Matsuda [13] and ours, respectively.

The measured wavelengths of ripples of ice produced in 10 hours on the round stick for $Q = 100, 200$ and 300 ml/h and the gutter on a plane at $\theta = \pi/2$ for $Q = 55, 100, 150, 200, 250$ and 300 ml/h are shown by \bullet and \blacksquare in Fig. 8, respectively. The theoretical dependence of the wavelength of ripples on various Q/l at $\theta = \pi/2$ is shown in Fig. 8 by the solid and dashed lines. The solid line is the numerical result with no approximation, while the dashed line is obtained from the approximate formula $\lambda = 2\pi(a^2 h_0 Pe_l / 3)^{1/3}$, with the replacement Q/l by $Q/l - (\rho_s / \rho_l) \bar{V} l_x$. Our theoretical results show that the wavelength increases gradually with an

increase in Q/l . The experimental results (● and ■) show weaker dependence of wavelength on Q/l than expected from the theoretical results, but qualitative behavior and the order of wavelength is almost the same.

In our experiment, the water supply rate Q from the top is kept constant. In the case of the gutter on a plane, the width l is constant. Therefore, the value of Q/l is not time dependent. However, in the case of ice produced on the round stick, the value of Q/l decreases as ice grows because the value of l increases with time t as $2\pi(R_0 + \bar{V}t)$ under the assumption that ice grows uniformly at \bar{V} , where R_0 is the radius of the stick. When plotting the values of wavelengths for ● in Fig. 8, we estimated the value of $l = 2\pi(R_0 + \bar{V}t)$ from $R_0 = 3$ mm, $\bar{V} = 1.7$ mm/h and $t = 10$ h.

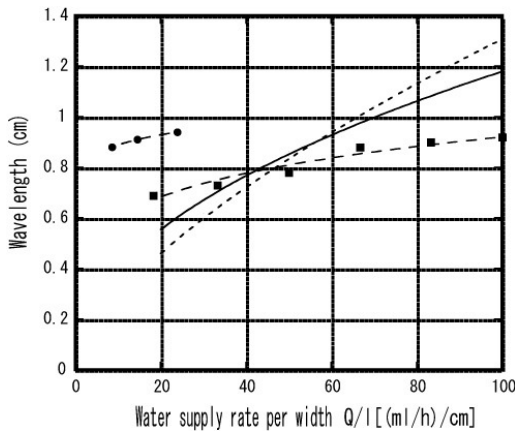


Fig. 8. The wavelength versus Q/l at $\theta = \pi/2$. Solid line: numerical results; dashed line: $\lambda = 2\pi(a^2h_0Pe_l/3)^{1/3}$ [10]; ●, ■: wavelength of ripples of ice produced on a round stick and gutter in 10 hours in our experiments, respectively.

As indicated in Fig. 4 (b), our theory predicts that ripples move upward with $v_{p*} = v_p / \bar{V} \approx 0.6$ at $Q = 200$ ml/h. When we use the measured value of $\bar{V} = 1.9$ mm/h at $Q = 200$ ml/h in Fig. 6 (d), $v_p \approx 1.14$ mm/h, the theoretical displacement is about 5.7mm for 5 hours. As shown by the white dashed lines in Fig. 9, all protruding parts on the right hand side of an icicle move upward. The measured mean displacements over 5 hours, shown in Fig. 8 is about 5 mm. This observation is consistent with the picture shown in Fig. 4 (c).

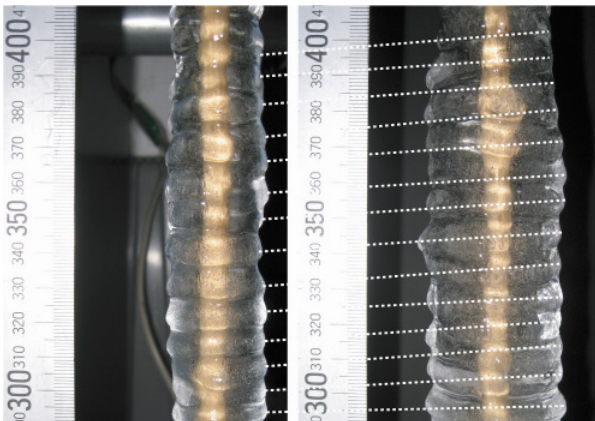


Fig. 9. Upward movement of ripples of ice produced on a 6 mm-diameter round stick, after time 5 (left) and 10 (right) hours at $Q = 200$ ml/h. The mean displacement of ripples is about 5 mm over 5 hours.

V. CONCLUSIONS

Two theoretical models for ripple formation mechanism on icicles developed in [6] and [8] were compared numerically based on our theoretical framework. We could not obtain the same results as the analytical results in model [6] despite solving the same governing equations with the same boundary conditions. Our numerical results obtained without employing the approximations used in model [8] were qualitatively in good agreement with our experimental results.

VI. ACKNOWLEDGMENTS

This work was carried out within the framework of the NSERC/Hydro-Quebec Industrial Chair on Atmospheric Icing of Power Network Equipment (CIGELE) and the Canada Research Chair on Engineering of Power Network Atmospheric Icing (INGIVRE) at Universite du Quebec a Chicoutimi. The authors would like to thank the CIGELE partners (Hydro-Quebec, Hydro One, Reseau Transport d'Electricite (RTE) and Electricite de France (EDF), Alcan Cable, K-Line Insulators, Tyco Electronics, Dual-ADE, and FUQAC) whose financial support made this research possible.

VII. REFERENCES

- [1] N. Maeno, L. Makkonen, K. Nishimura, K. Kosugi, and T. Takahashi, "Growth rates of icicles," *J. Glaciol.*, Vol. 40, pp. 319-326, 1994.
- [2] W. W. Mullins and R. F. Sekerka, "Morphological stability of a particle growing by diffusion or heat flow," *J. Appl. Phys.*, Vol.34, pp. 323-329, 1963.
- [3] J. S. Langer, "Instabilities and pattern formation in crystal growth," *Rev. Mod. Phys.*, Vol. 52, pp. 1-28, 1980.
- [4] B. Caroli, C. Caroli, and B. Roulet, "Instabilities of planar solidification fronts," in *Solids Far From Equilibrium*, edited by C. Godreche, Cambridge : Cambridge University Press, 1992.
- [5] T. B. Benjamin, "Wave formation in laminar flow down an inclined plane," *J. Fluid Mech.*, Vol. 2, pp. 554-574, 1957.
- [6] N. Ogawa and Y. Furukawa, "Surface instability of icicles," *Phys. Rev. E*, Vol. 66, 041202, 2002.
- [7] P. Schewe and J. Riordon, "Icicle ripples," *Physics Update, Physics Today*, January p.9, 2003.
- [8] K. Ueno, "Pattern formation in crystal growth under parabolic shear flow," *Phys. Rev. E*, Vol. 68, 021603, 2003.
- [9] K. Ueno, "Pattern formation in crystal growth under parabolic shear flow II," *Phys. Rev. E*, Vol. 69, 051604, 2004.
- [10] K. Ueno, "Characteristics of the wavelength of ripples on icicles," *Phys.Fluids*, Vol. 19, 093602, 2007.
- [11] L. D. Landau and E. M. Lifschitz, *Fluid Mechanics*, London: Pergamon Press, 1959.

- [12] K. Ueno and M. Farzaneh, "The Effect of Airflow on the Wavelength of Ripples on Icicles," in *Proc. of 13th International Workshop on Atmospheric Icing on Structures*, Andermatt, Switzerland, 2009.
- [13] S. Matsuda, "Experimental study on the wavy pattern of icicle surface", Master's thesis, Institute of Low Temperature Science, Hokkaido University, 1997.